PAPER

Ultrathin Ni(OH)$_2$ nanosheets: a new strategy for cocatalyst design on CdS surfaces for photocatalytic hydrogen generation

Liqun Mao,[ab] Qianqian Ba,[a] Xinjia Jia,[a] Shuang Liu,[a] Heng Liu,[a] Jing Zhang,[a] Xiying Li [ID][a] and Wei Chen [ID]*[a]

Ultrathin metal materials exhibit quantum size and surface effects that give rise to unique catalytic properties. In this paper, we report a facile liquid synthesis method for polyvinylpyrrolidone (PVP, K30) capped ultrathin Ni(OH)$_2$ nanosheets with lamellar structure. The as-prepared ultrathin Ni(OH)$_2$ nanosheets coupled with CdS nanorods exhibit excellent activity in hydrogen generation from water splitting under visible light. The H$_2$ evolution rate of Ni(OH)$_2$/CdS, 40.18 mmol h^{-1} g$_{Cat.}^{-1}$ with a quantum efficiency of 66.1% at 420 nm, is *ca.* 1.5 times that of Pt/CdS with an optimal loading amount (1.25 wt%) under the same reaction conditions. Considering the cost of photocatalysts, the ultrathin Ni(OH)$_2$ nanosheet coupled CdS photocatalyst may have a promising commercial application in photocatalytic hydrogen production.

1. Introduction

Hydrogen production from water splitting is considered the "Holy Grail" of the hydrogen economy, and has been actively studied in recent decades. The efficiency of any solar water splitting photocatalyst depends upon its ability to utilize solar radiation and its photochemical conversion efficiency. Therefore, considerable efforts have been focused on developing visible-light-driven photocatalysts, such as limited mixed oxides, (oxy)nitrides, and (oxy)sulfides, capable of using abundant visible light (λ > 420 nm). Moreover, the loading of noble metal cocatalyst, such as Pt, Pd, Ru, and Rh, is widely accepted in theory and experimental research for hydrogen production from water splitting since these cocatalysts can trap photogenerated electrons and catalyze the H$_2$ evolution reaction, and thus significantly improving the performance of the semiconductor photocatalyst. However, their application in large-scale energy production are inhibited due to the scarcity and high costs of these noble metals. In this regard, the exploitation of noble-metal-free materials with low costs, high efficiencies and good durability as cocatalysts for photocatalytic H$_2$ production is highly desirable.

Recently, metallic nickel[1–12] and nickel compounds (*e.g.* NiO,[13–21] NiS,[22–36] Ni(OH)$_2$,[37–42] and Ni@C/CdS[43]) were reported to function as cocatalysts for water splitting affording hydrogen

and oxygen or for organic pollutant degradation in water and air. Rong Xu and You Xu have given a comprehensive review about Ni-based cocatalysts for semiconductor-based photocatalytic H$_2$ production.[44] Among these metallic nickel and nickel compounds, Ni(OH)$_2$ cocatalysts have been widely applied to combine with various semiconductors for efficient photocatalytic H$_2$ production. It can promote the electron transfer at the interface with primary catalysts and catalyze the H$_2$ evolution.

It is well recognized that several key factors, including the loading amount, phase, structure and size, determine the activities of cocatalysts when combining with semiconductors for photocatalytic H$_2$ production. Qiao *et al.* prepared Ni-based cocatalysts, such as NiO, NiS, Ni(OH)$_2$ and Ni, and loaded them onto the surface of Zn$_x$Cd$_x$S, the hydrogen generation results demonstrated that the Ni(OH)$_2$ loaded Zn$_x$Cd$_x$S exhibited a very high photocatalytic hydrogen generation rate of 7160 μmol h^{-1} g^{-1}, which is due to the synergetic effect between Ni(OH)$_2$ and metallic Ni formed *in situ* during the photocatalytic reaction.[37] Huang *et al.* synthesized (Ni(OH)$_2$/g-C$_3$N$_4$) photocatalysts by a simple precipitation method, and found that the hydrogen generation activity of C$_3$N$_4$ loaded with 0.5 mol% Ni(OH)$_2$ under visible light (λ > 420 nm) was even higher than that of the one loaded with 1 mol% Pt.[38] Shangguan *et al.* prepared β-Ni(OH)$_2$ modified TaON *via* a precipitation method. With methanol solution (10%, v/v) acted as sacrificial electron donor, they investigated the dosage of Ni(OH)$_2$ NPs in the presence of water soluble TaON under visible light (λ > 420 nm) on the hydrogen generation activity. And the highest efficiency obtained with Ni(OH)$_2$ NPs loading of 5% reached up to 2 times of Pt/TaON. They suggested that the rapid electrons migration from CB of

[a]*Henan Engineering Research Center of Resource & Energy Recovery from Waste, Henan University, Kaifeng 475004, PR China. E-mail: chanwee@henu.edu.cn; Tel: +86 15737821275*

[b]*Institute of Functional Polymer Composites, Henan University, Kaifeng 475004, PR China*

TaON to $Ni(OH)_2$ that restrained the recombination of charge carriers generated by TaON, and finally facilitated the hydrogen evolution.[40] Wang *et al.* employed a novel method to enhance the interaction between the $Ni(OH)_2$ and HNb_3O_8, and the synthesized $Ni(OH)_2$ had an smaller size, furthermore, the optimal H_2 generational rate of sample is about 15.7 times than that of the $Ni(OH)_2$ prepared by a traditional deposition method. They suggested that the smaller size of cocatalyst could provide a larger number of surface active sites and improved the photocatalytic hydrogen evolution performance.[42]

Recent decade, ultrathin metal-based materials were found owning quantum size and surface effects, and could give rise to unique physical and chemical properties. By far, only a few metal ultrathin materials have been reported, such as surfactant-capped Pd, Rh, and Ru nanoplates.[45–47] In this paper, we applied a facile liquid method to synthesize $Ni(OH)_2$ with ultrathin nanosheets structure, and used it as cocatalyst for hydrogen generation from water splitting. Ultrathin $Ni(OH)_2$ nanosheets coupled with CdS nanorods photocatalyst exhibits excellent photocatalytic hydrogen generation activity under visible light, the hydrogen generation rate reaches to $40.18 \text{ mmol h}^{-1} \text{ g}^{-1}$ (QE = 66.1% at 420 nm), much more higher than that of Pt/CdS ($26.8 \text{ mmol h}^{-1} \text{ g}^{-1}$) with optimal loading amount (1.25 wt%) under the same reaction conditions.

2. Experimental section

All chemicals were used without further purification. Chloroplatinic acid ($H_2PtCl_6 \cdot 6H_2O$) was obtained from Reagent No. 1 Factory of Shanghai Chemical Reagent Co., Ltd. Sodium borohydride ($NaBH_4$) was obtained from Chinese Sinopharm Chemical Reagent Co. Ltd. Polyvinylpyrrolidone (PVP, K30) was obtained from BASF. $Cd(NO_3)_2 \cdot 4H_2O$, NH_2CSNH_2, $NiCl_2 \cdot 6H_2O$ (Kermel Chemical Reagent Co. Ltd.) and absolute alcohol (Ante Biotech Co. Ltd.) were used as starting materials. The water used in the preparation was distilled water.

2.1 Preparation of ultrathin $Ni(OH)_2$ nanosheets coated CdS nanorods

Ultrathin $Ni(OH)_2$ nanosheets was synthesized *via* chemical reduction route. 0.48 mL 0.04259 mol L^{-1} $NiCl_2$ and 6 drops PVP (0.1 wt%) was added into 9 mL distilled water, mixed under stirring for 1–2 min, and then 0.06349 mol L^{-1} $NaBH_4$ was added into the solution drop by drop until the solution changed to grey black.

CdS nanorods served as photocatalyst were prepared by a solvothermal method.[48] 48 mL of 1,2-ethylenediamine(en), 3.1537 g of $Cd(NO_3)_2 \cdot 4H_2O$ (Kermel Chemical Reagent Co. Ltd., China) and 2.3040 g of NH_2CSNH_2 (Kermel Chemical Reagent Co. Ltd., China) were added to a beaker, and reacted under stirred at room temperature for 30 min, then it was transferred into a sealed Teflon-lined autoclave, and was kept at 160 °C for 48 h. The so-obtained yellow product was separated from the solution, washed with distilled water and absolute alcohol, dried under 313 K for 24 h in a vacuum furnace, finally ground and stocked in an airtight vial. The as-prepared CdS with

nanorods structure belongs to hexagonal phase, and possessed a large BET surface area of $36.7 \text{ m}^2 \text{ g}^{-1}$.

The as-obtained ultrathin $Ni(OH)_2$ nanosheets was mixed with 0.1 g of CdS nanorods under stirring for water splitting-hydrogen generation reaction. During the water splitting reaction process, ultrathin $Ni(OH)_2$ nanosheets was deposited on CdS surface with the assistance of photo-induced electrons.

2.2 Characterization

Crystalline structure of as-prepared ultrathin $Ni(OH)_2$ nanosheets was determined by using powder X-ray diffraction (XRD) (Philips X'Pert Pro, Netherlands) with Cu Kα radiation. The applied current and voltage were 40 mA and 40 kV, respectively. The grain size and microstructure of ultrathin $Ni(OH)_2$ nanosheets were analyzed with a field emission transmission electron microscope (TEM) (FEI TalosF200S, USA). Scanning transmission electron microscopy coupled with electronic differential system (STEM-EDX) (FEI Tecnai G2 F20 S-TWIN, USA) were used to investigate the distribution of $Ni(OH)_2$ NPs on the surface of CdS nanorods. The UV-vis diffuse reflection spectra (DRS) of $Ni(OH)_2$/CdS were determined by a UV-vis spectrophotometer (Shimadzu UV-2450, Japan) and were converted to absorbance by the Kubelka–Munk method. PL spectra and lifetime of $Ni(OH)_2$/CdS were recorded using a FLS 980 (Edinburgh analytical instruments, UK) furnished by a 450 W xenon lamp and a μF900H high-energy microsecond flash lamp as the excitation source. The Fourier transformation infrared spectrometer (FT-IR) (Nicolet AVATAR 360, USA) was used to analyze forming mechanism of the ultrathin $Ni(OH)_2$ nanosheets.

2.3 Evaluation of photo-catalytic activity

A water-jacketed stainless vessel (diameter 14.0 cm, height 10.0 cm) fitted with a quartz window (diameter 7.0 cm, exposed area 38 cm^2) was used as the photo-reactor. The reaction temperature was maintained at 311 ± 2 K by circulating isothermal water in the water jacket of the photo-reactor. A 300 W Xe lamp (Beijing Perfect light Company; Beijing, China) equipped with a cut-off filter ($\lambda > 420$ nm) was used as the light source. Before photo-catalytic reaction was commenced, 0.1 g of CdS nanorods photocatalyst was adequately well mixed with the ultrathin $Ni(OH)_2$ nanosheets, then the slurry was added into 1 M $(NH_4)_2SO_3$ aqueous solution, and the total volume of the reaction solution was kept at 50 mL. The solution was purged with N_2 flow (>99.999%) for 30 min under stirring, and so the ultrathin $Ni(OH)_2$ nanosheets might get well contact with CdS nanorods photocatalyst.

3. Results and discussion

3.1 Structure characterization of ultrathin $Ni(OH)_2$ nanosheets

Fig. 1a shows XRD pattern of as-prepared $Ni(OH)_2$ NPs. It's seen that there is no clear diffraction peak within 30–70°, indicating $Ni(OH)_2$ NPs being of poor crystallinity. The diffraction peaks located at 39.8°, 42.2°, 44.8°, and 59.4° could be attributed to
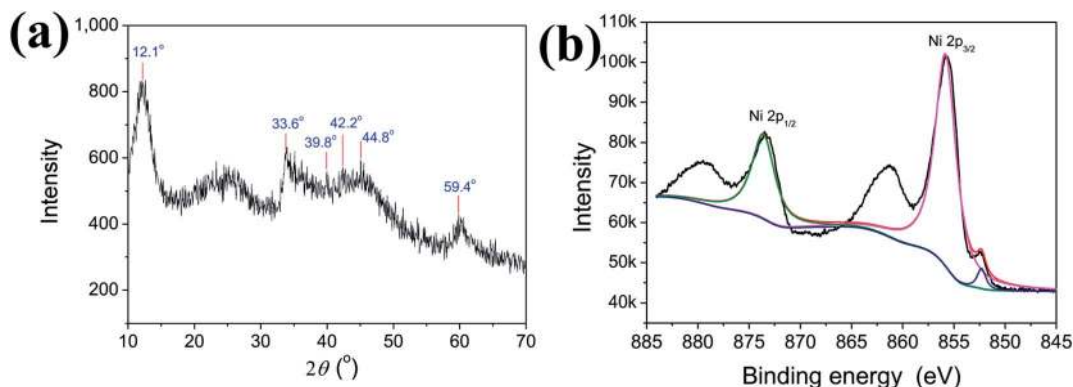
Fig. 1 XRD spectrum (a) and XPS spectra (b) of as-prepared Ni(OH)$_2$ NPs.

Ni(OH)$_2$ NPs (JCPDS card no. #45-1027), while the diffraction peak located at 33.6° could be attributed to Ni(OH)$_2$ (JCPDS card no. #14-0117). All of the diffraction peaks slightly change towards high degree, which might be caused by surface modified PVP. Moreover, there is a strong and broaden peak centered at 12.1°, indicating the lamellar structure of the as-prepared Ni(OH)$_2$ NPs. To further investigate the Ni chemical state and XPS was employed, the result was shown in Fig. 1b. It can be found that two strong peaks at 855.8 eV and 873.6 eV are indexed to Ni 2p$_{3/2}$ and Ni 2p$_{1/2}$, suggesting Ni exists in the form of hydroxide on the surface. And the peaks observed at 852.3 eV can be ascribed to metallic Ni, which is consistent with the XRD synthesis. To sum up, we think that the as-prepared Ni NPs mainly consist of Ni(OH)$_2$ and very small amount of metallic Ni as well. It's generally believed that Ni is more active. In this case, Ni NPs was synthesized *via* chemical reduction in the aqueous solution, and its surfaces unavoidable to be oxidized, and further combined with H$_2$O to form Ni(OH)$_2$.

Fig. 2a and b are the TEM and HRTEM image of as-prepared Ni(OH)$_2$ NPs, respectively. It is clearly seen that the so-obtained Ni(OH)$_2$ NPs shows irregular ultrathin nanosheets with lamellar structure, highly identify with the testing result of XRD. As can be seen, the ultrathin Ni(OH)$_2$ nanosheets with lamellar structure is considerably uniform and well dispersed. In addition, the ultrathin Ni(OH)$_2$ nanosheets is of high yield, no obvious other morphology was detected. Fig. 2c is the enlarged image of the red square in Fig. 2b, which gives more details about the laminar nanosheets. The average thickness of single sheet and interlamellar spacing are estimated to be 0.187 nm and 0.193 nm, respectively. The thickness of single sheet is close to the radius of Ni mono-atom (0.1243 nm), so we suggest that the nanosheets is properly monoatomic layer. Fig. 2d is the selected area electron diffraction (SAED), showing the dispersing diffraction ring, which indicate that the particle is composed of extremely fine particles, with poor crystallinity. And the SAED result is also consistence with XRD (Fig. 1).

FT-IR analysis of the as-prepared metallic Ni(OH)$_2$ NPs was applied to investigate the formation mechanism of its ultrathin nanosheets structure. As shown in Fig. 3 curve b, the absorption peaks at 2960 cm^{-1} and 1430 cm^{-1} are due to the ν_{C-H} and δ_{C-H} of PVP molecular, respectively. The peaks located at 1373 cm^{-1}

and 1292 cm^{-1} are consistent with symmetric and asymmetric stretching vibration of C–N. The peak at 1660 cm^{-1} is according to $\nu_{C=O}$. The absorption of water, observed at 3452 cm^{-1}, is identical to ν_{O-H}. All of these typical absorption peaks of PVP molecular could be seen in curve a, which confirmed that PVP was decorated on the surface of ultrathin Ni(OH)$_2$ nanosheets. In addition, the absorption peaks attributed to $\nu_{C=O}$ in Fig. 4a is seen at 1630 cm^{-1}, changing towards low wavenumber, indicating the formation of C=O$\cdots$Ni^{2+}.[49] Therefore, we argued that the precursor Ni^{2+} combined with C=O to form C=O$\cdots$Ni^{2+} during the previous dispersing process, and then Ni^{2+} was reduced by NaBH$_4$ to give birth of Ni crystal seed. PVP is a perfect membrane-forming agent, and was served as a capping reagent in reduction reaction, so the Ni(OH)$_2$ NPs with ultrathin nanosheets structure was yielded under the directing function of PVP. In this work, ultrathin Ni(OH)$_2$ nanosheets shows lamellar structure, which were also observed by several research groups. Zheng *et al.* reported a general CO-confined growth method to prepared hexagonal palladium nanosheets.[45] The average thickness of the as-prepared nanosheets was found to be 1.8 nm-less than 10 atomic layers thick, and as the concentration of palladium nanosheets increasing, the nanosheets had the trend to assemble into an extended lamellar structure in the presence of CTAB. Yan *et al.* synthesized Ru triangular and irregular nanoplates by means of hydrothermal method, they also found that Ru nanoplates could bend and assemble into layered structures in a face-to-face manner on the carbon membranes of the copper grid.[46] We think that several factors such as the concentration of precursor, solvent, capping reagent and surfactant, might led to the lamellar structure.

3.2 The deposition of ultrathin Ni(OH)$_2$ nanosheets on surface of CdS nanorods

As described in experimental section, ultrathin Ni(OH)$_2$ nanosheets was prepared *via* chemical reduction with PVP as soft template. The so-obtained ultrathin Ni(OH)$_2$ nanosheets was mixed with CdS nanorods photocatalyst under anoxic condition, and then deeply reduced by the photo-generated electrons of CdS with (NH$_4$)$_2$SO$_3$ as sacrificial agent. In order to determine the distribution of Ni(OH)$_2$ nanosheets on the surface of CdS nanorods, STEM analysis was performed and the images are
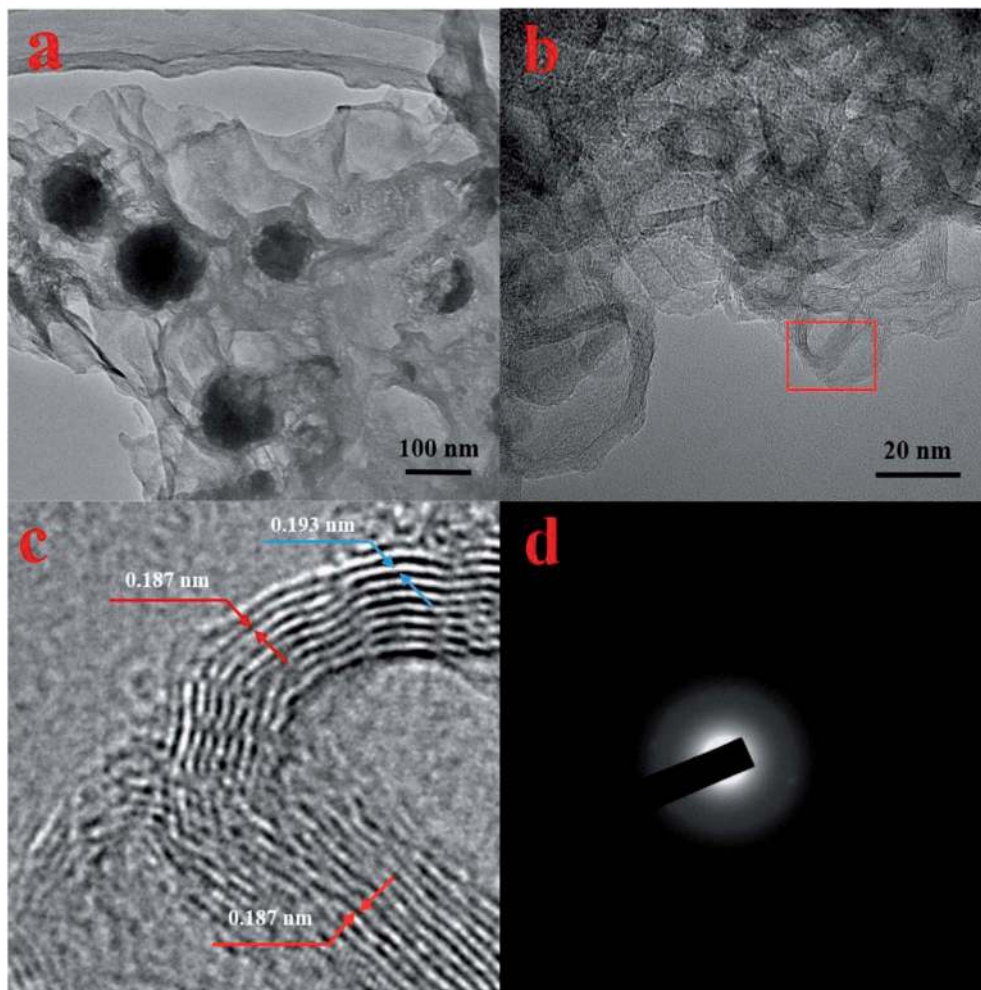
Fig. 2 HRTEM images (a) and (b), enlarged image (c), and SAED pattern (d) of as-prepared ultrathin Ni(OH)$_2$ nanosheets.
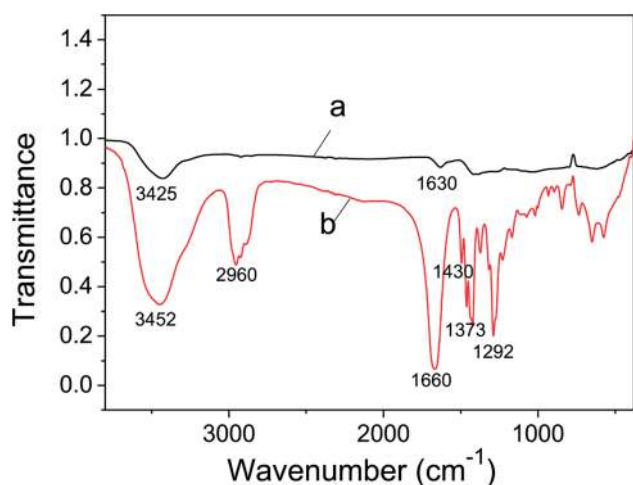

Fig. 3 FT-IR spectra of as-prepared ultrathin Ni(OH)$_2$ nanosheets (a) and PVP (b).

shown in Fig. 4. The HAADF image of Ni(OH)$_2$/CdS shows that there is no obvious Ni(OH)$_2$ nanosheets detected on the surface of CdS nanorods (Fig. 4a). In addition, the elemental mapping

of Ni (Fig. 4d, g and h) indicates that Ni(OH)$_2$ nanosheets concentrate on the surface of CdS nanorods, and well distribute on the most surface of CdS nanorods. So far, such extensive distribution of cocatalyst on the surface of photocatalyst is rarely studied. Usually, the concerned cocatalysts no matter what they are, scattered on the surface of photocatalyst, especially when the loading amount of cocatalyst is low as shown in this case (1.20 wt%).

Fig. 5a and b show the XRD patterns of CdS and ultrathin Ni(OH)$_2$ nanosheets decorated CdS, respectively. All diffraction peaks of CdS nanorods can be indexed to the hexagonal CdS phase (space group: $P6_3mc$; JCPDS card no. 41-1049), and no other characteristic peaks of impurities were detected. Moreover, there is no characteristic peak of Ni(OH)$_2$ nanosheets found in Fig. 5b, which might be due to the low loading capacity of Ni(OH)$_2$ on CdS surface.

Moreover, it's not difficult to find an obvious difference *via* comparing the XRD patterns of CdS and Ni(OH)$_2$/CdS, *i.e.* the peak intensity of most crystal planes changes a lot. The relative peak intensity of each crystal plane was calculated and listed in Table 1. As can be seen, the peak intensity of crystal planes (200), (110), (100) and (002) decreased, while the peak intensity of crystal planes (103), (101), (112) increased. The investigating
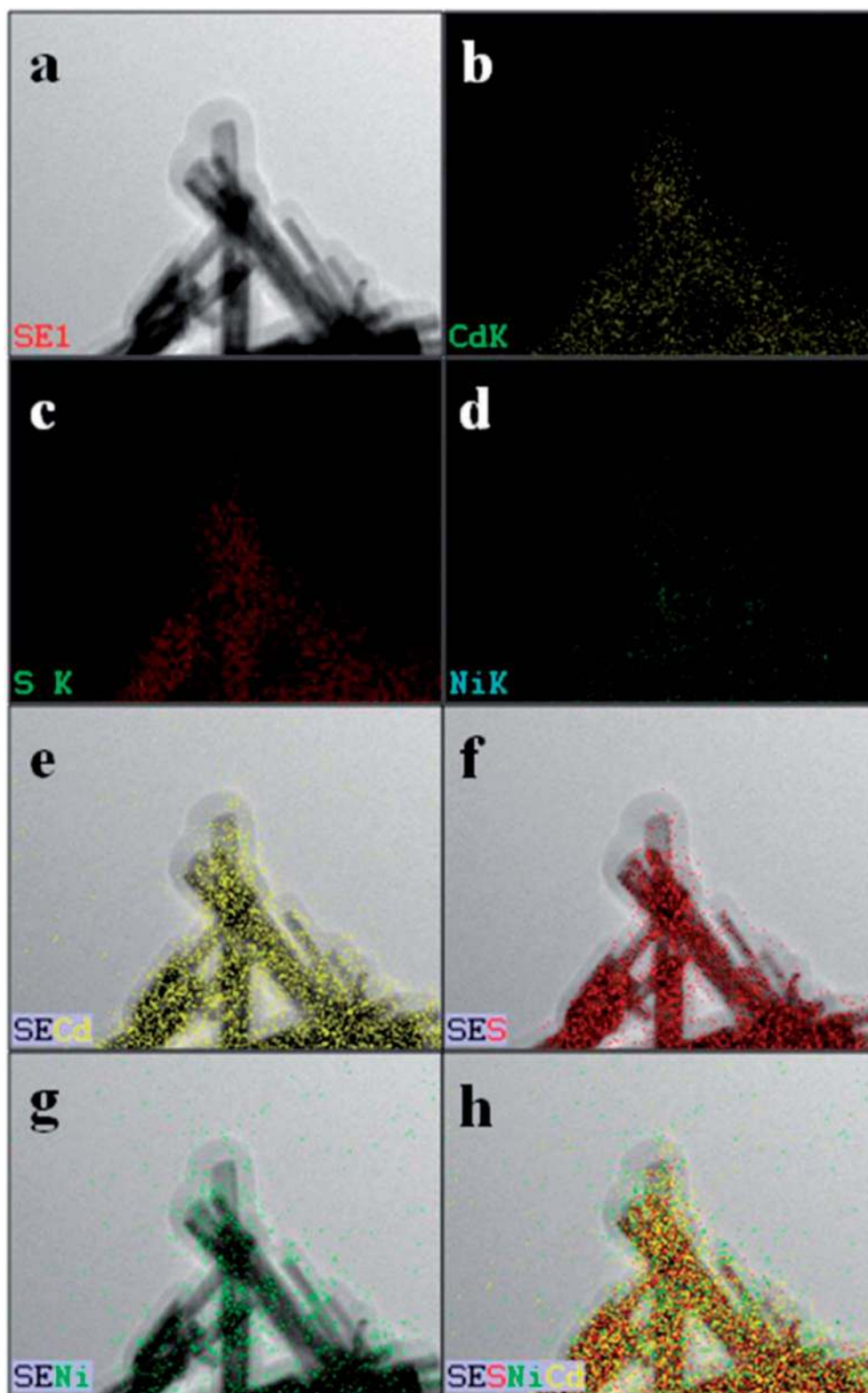
Fig. 4 HAADF-STEM image of $Ni(OH)_2/CdS$ ($Ni(OH)_2$ loading amount is 5 wt%) (a), along with the corresponding elemental maps (b–h).

result revealed that the photo-induced deposition of ultrathin $Ni(OH)_2$ nanosheets on the surface of CdS nanorods has orientations. Ultrathin $Ni(OH)_2$ nanosheets trends to load on the crystal planes (200), (110), (100) and (002), which reduces the exposal opportunity of these crystal planes, and thus causes the decreasing of peak intensity. The orientation deposition of ultrathin $Ni(OH)_2$ nanosheets on CdS nanorods properly relates to the transfer mechanism of photo-induced carriers inside the
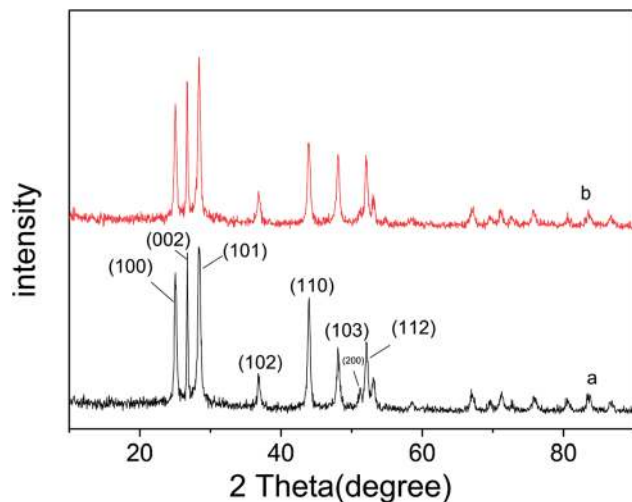
Fig. 5 XRD spectra of CdS (a) and Ni(OH)$_2$/CdS (b).

Fig. 6 UV-vis spectra of CdS (a) and Ni(OH)$_2$/CdS (b).

semiconductor. And intensive investigations are necessary to reveal the relationship between the electron transfer and the structure of photocatalyst semiconductor.

3.3 Spectra analyses

UV-vis diffuse reflectance spectra (DRS) of CdS nanorods and Ni(OH)$_2$/CdS were shown in Fig. 6. They displayed that the absorption threshold and band gap of CdS were about 523 nm and 2.4 eV respectively, and remained unchanged as ultrathin Ni(OH)$_2$ nanosheets loaded on its surface *via* photo-induced hydrogen generation reaction. Moreover, compared with CdS nanorods, the absorbance of Ni(OH)$_2$/CdS decreased in the testing region 200–523 nm and increased within 523–900 nm, which might be caused by the coating of ultrathin Ni(OH)$_2$ nanosheets on the surface of CdS nanorods.

Fig. 7 shows the photoluminescence (PL) spectra of as-synthesized CdS nanorods and Ni(OH)$_2$/CdS measured at room temperature at an excitation wavelength of 407 nm. As-synthesized CdS (Fig. 7a) exhibits two strong emission peaks at 440–460 nm and 506 nm, respectively. The former emission peak is caused by band-edge emission, while the latter is usually attributed to surface-defect emission. However, as ultrathin Ni(OH)$_2$ nanosheets was deposited on as-prepared CdS surface
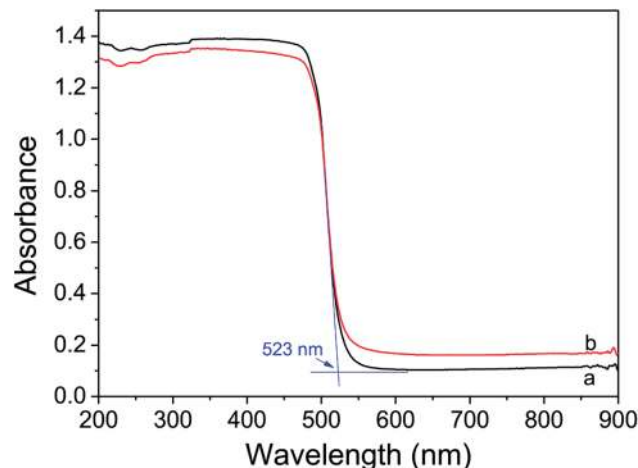
(Fig. 7b), the intensity of the two peaks decreased significantly, which indicated that the recombination of photo-generated charges was repressed somehow.

The lifetime curves of the photocatalysts after hydrogen generation reaction were monitored under the excitation at 407 nm (Fig. 8). It's seen that lifetime curve of Ni(OH)$_2$/CdS has a clearly delay, which indicates that the lifetime of the photo-generation electrons is prolonged. All of the curves could be well fitted to a double exponential function [$I = \alpha_1 \exp(-t/\tau_1) + \alpha_2 \exp(-t/\tau_2)$], based on which the lifetime value (τ_1, τ_2), and the pre-exponential factor (α_1, α_2) were calculated (Table 2). In addition, the average lifetime value (τ_{ave}) could be calculated by the function [$\tau_{ave} = (\alpha_1\tau_1^2 + \alpha_2\tau_2^2)/(\alpha_1\tau_1 + \alpha_2\tau_2)$] (Table 2). Table 2 clearly showed that the short (τ_1) and long lifetime (τ_2) of CdS and Ni(OH)$_2$/CdS were 8455.56 ns, 10 882.96 ns, and 883.76 ns, 876.81 ns, respectively. The short lifetime (τ_1) of Ni(OH)$_2$/CdS was much higher than that of CdS alone.

Generally, the short lifetime τ_1 was caused by the recombination of photo-induced carriers in the bulk of the photocatalyst CdS, while the long lifetime τ_2 could be explained by the

Table 1 XRD data comparison of CdS and Ni(OH)$_2$/CdS photocatalysts

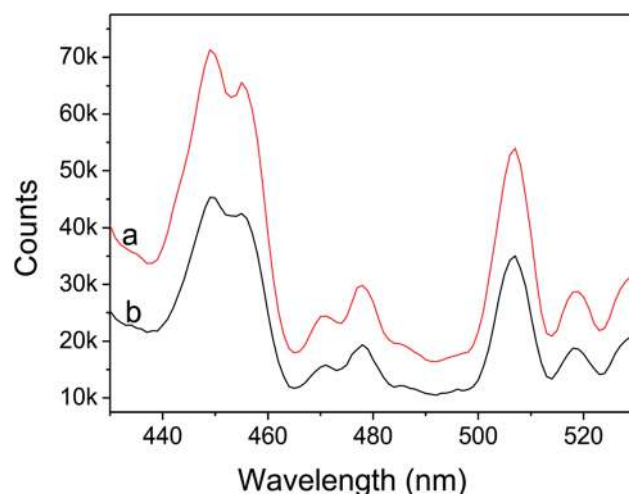| $2\theta/(°)$	Lattice plane	I		$I_{Ni(OH)_2/CdS}/I_{CdS}$
		CdS	Ni(OH)$_2$/CdS	
25.03	(100)	250	222	0.888
26.72	(002)	278	257	0.925
28.33	(101)	295	310	1.051
36.92	(102)	64	62	0.969
43.96	(110)	218	158	0.725
48.06	(103)	122	137	1.123
51.06	(200)	39	16	0.410
52.15	(112)	128	133	1.039
53.00	(201)	57	56	0.982

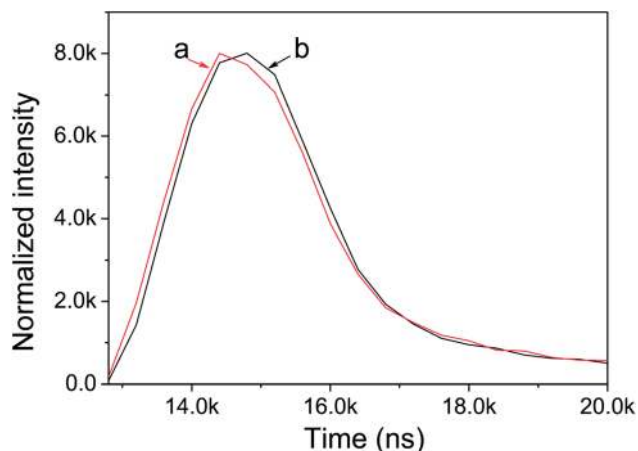Fig. 7 PL spectra of CdS (a) and Ni(OH)$_2$/CdS (b), monitored under the excitation at 407 nm.

Fig. 8 Fluorescence lifetime of CdS (a) and $Ni(OH)_2$/CdS (b) photocatalyst, monitored under the excitation at 407 nm.

recombination of photo-induced carriers on its surface. The lifetime of semiconductor photocatalyst was closely associated with the separation and transformation of the photo-induced carriers.[50–53] Increasing lifetime can enhance the separation efficiency between photo-induced electrons and holes, resulted in the promotion of photocatalytic hydrogen generation rate. Therefore, we suggest that ultrathin $Ni(OH)_2$ nanosheets coated CdS largely inhibited the combination of photo-generated carriers.

3.4 Hydrogen evolution properties

Fig. 9 shows the H_2 evolution rate (γ_{H_2}) of CdS modified with ultrathin $Ni(OH)_2$ nanosheets, and the inset figure directly gives the H_2 evolution rate of each photocatalyst when its activity gets stable. CdS alone is inactive, and almost no hydrogen was detected. It's seen that $Ni(OH)_2$/CdS photocatalyst shows high activity in H_2 evolution from water-splitting under visible light. And as loading amount of ultrathin $Ni(OH)_2$ nanosheets increased within 1.0–2.0 wt%, the H_2 evolution rate of $Ni(OH)_2$/CdS increased in the beginning, reached to its peak value 40.18 mmol h^{-1} g^{-1} (QE = 66.1%, λ = 420 nm) as loading amount equals to 1.2 wt%, and then slightly decreased.

In order to get a technical evaluation of this work, H_2 evolution reaction was performed in presence of Pt/CdS under the same reaction conditions (Fig. 10). Pt NPs with a particle size of 5 nm was synthesized by means of chemical reduction with chloroplatinic acid hydrate used as precursor, sodium borohydride as reducer. The experimental testing result indicates that H_2 evolution rate of Pt/CdS with optimal loading amount (1.25 wt%) reaches to 26.80 mmol h^{-1} g^{-1} (QE = 13.3%,
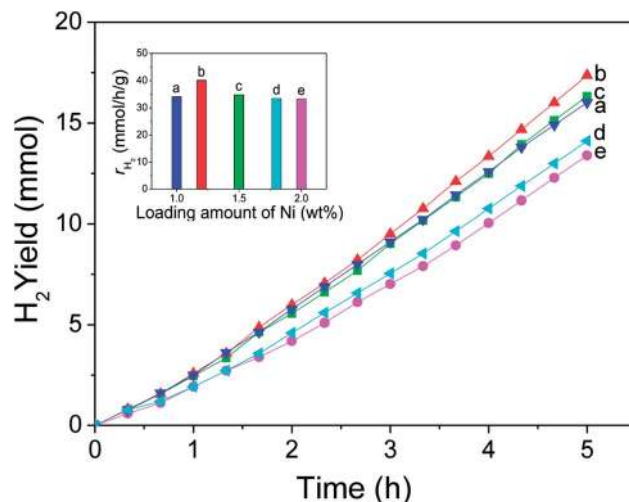

Fig. 9 H_2 evolution rate under visible light (λ > 420 nm) in the presence of $Ni(OH)_2$/CdS photo-catalyst. Reaction conditions: a 300 W Xe lamp equipped with a cut-off filter (λ > 420 nm), 50 mL 1 mol L^{-1} (7.5 g/ 50 mL) $(NH_4)_2SO_3$ aqueous solution, 0.1 g $Ni(OH)_2$/CdS photocatalyst, reaction temperature is ca. 311 ± 2 K.

λ = 420 nm). Curves a–d were obtained with the same Pt loading amount (1.25 wt%) and under the same reaction conditions, and the result showed good repeatability.

The stability of $Ni(OH)_2$/CdS was also investigated and the result was shown in Fig. 11. Due to the high hydrogen generation rate, the sacrificial agent $(NH_4)_2SO_3$ was almost consume away after one cycle. And therefore, 6.0 g sacrificial agent $(NH_4)_2SO_3$ and 1.5 mL H_2O were added into the reaction solution, and the solution was purged with N_2 flow (>99.999%) for 30 min again before reaction. According to the inset figure in Fig. 11, the hydrogen generation rate for the five cycles are 40.78, 42.04, 37.79, 37.79, 35.28 mmol h^{-1} g^{-1}, respectively. The total amount of hydrogen produced in 25 h reaches to 96.84 mmol, in other words, the production capacity of

Table 2 Results of double-exponential fitting to the fluorescence of CdS and $Ni(OH)_2$/CdS

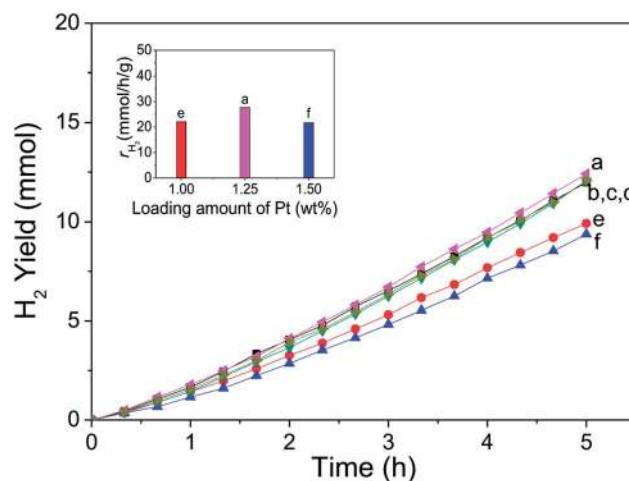| Sample	τ_1 (ns)	α_1 (%)	τ_2 (ns)	α_2 (%)	τ_{ave} (ns)
$Ni(OH)_2$/CdS	10 882.96	55.11	876.81	44.89	10 266.73
CdS	8455.56	45.28	883.76	54.72	7606.43

Fig. 10 H_2 evolution rate under visible light (λ > 420 nm) in the presence of Pt/CdS photo-catalyst. Reaction conditions: a 300 W Xe lamp equipped with a cut-off filter (λ > 420 nm), 50 mL 1 mol L^{-1} (7.5 g/ 50 mL) $(NH_4)_2SO_3$ aqueous solution, 0.1 g Pt/CdS photocatalyst, reaction temperature is ca. 311 ± 2 K.
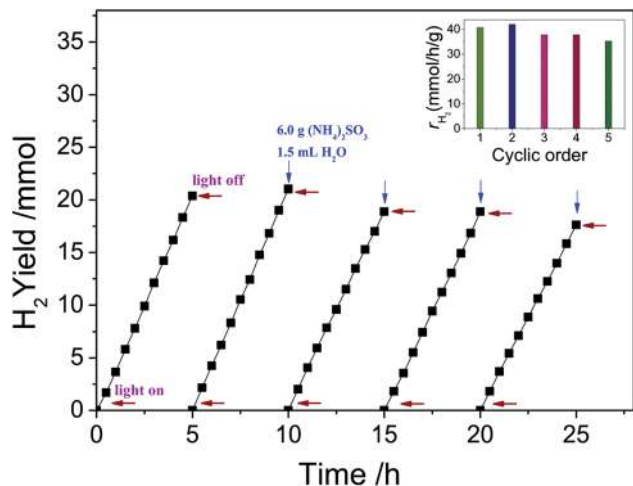
Fig. 11 The stability of Ni(OH)$_2$/CdS photo-catalyst. Reaction conditions: A 300 W Xe lamp equipped with a cut-off filter ($\lambda > 420$ nm), 50 mL 1.3 mol L^{-1} (10.0 g/50 mL) (NH$_4$)$_2$SO$_3$ aqueous solution, 0.1 g Ni(OH)$_2$/CdS photocatalyst, reaction temperature is ca. 311 ± 2 K.

hydrogen is 1.735 m^3 h^{-1} m^{-3} reaction solution, while the raw material cost of photocatalyst is less than 2\$. In short, ultrathin Ni(OH)$_2$ nanosheets cocatalyst coupled with CdS nanorod photocatalyst has huge application prospects.

3.5 Discussion

To compare the two cocatalysts, the hydrogen generation rate of ultrathin Ni(OH)$_2$ nanosheets coated CdS nanorods is 1.5 times as much as that of Pt/CdS, which is a so excited result. It's generally thought that quantum efficiency mainly depends on three aspects, *i.e.* the absorption efficiency of photocatalyst to the injected light, the separation and transfer efficiency of photo-induced charges in the bulk and surface of photocatalyst, and the catalytic evolution of H$_2$ and O$_2$. Therefore, far more works focus on the three steps in order to push forward the application of photo-catalytic technique in H$_2$ evolution from water splitting. Fig. 12 gives a schematic of the electrons transfer and capture by Ni(OH)$_2$ NPs cocatalyst on the surface of CdS nanorods. The potential of Ni^{2+}/Ni (Ni^{2+} + 2e$^-$ = Ni, E° = -0.23 V) is less negative than the conduction band (CB) (-0.7 V) of CdS, which favors the transfer of CB electrons from CdS to Ni(OH)$_2$, and finally prolong the lifetime of them, which is confirmed by the fluorescence lifetime testing (Fig. 8).

Moreover, it's thought that 2D nanostructures could exhibit fascinating properties, such as high electron mobility, quantum Hall effects, extraordinary thermal conduction, magnetic resonant mode, superconductivity, and catalytic properties.[45–47,54–57] As mentioned above, our research group had investigated the photocatalytic properties of Ni(OH)$_2$ NPs coupled with CdS nanorods towards hydrogen generation from water splitting. Ni(OH)$_2$ nanoparticles were prepared *via* chemical reduction of aqueous NiCl$_2$·6H$_2$O by N$_2$H$_4$·H$_2$O, and loaded on the surface of CdS nanorods by photo-induced electrons as did in this case.[5] The as-obtained Ni(OH)$_2$ nanoparticles with an average size of about 10 nm have face centered cubic structure, and provided a hydrogen production rate of 25.848 mmol (h^{-1} g^{-1}) (QE =
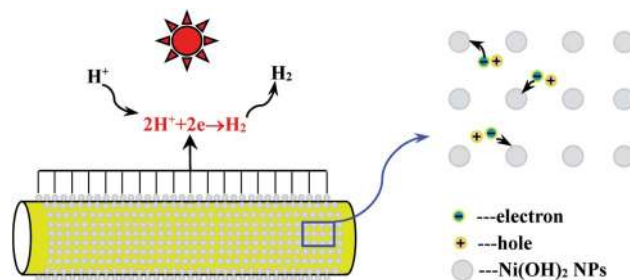

Fig. 12 Electrons capture by ultrathin Ni(OH)$_2$ nanosheets on the surface of CdS nanorod.

26.8%, $\lambda = 420$ nm) under the same reaction system. Therefore, we argued that 2D nanostructures with atomic thickness may expose specific crystal planes to the largest extent so that they may show enhanced co-catalytic properties. Acted as electron trapping centers, ultrathin Ni(OH)$_2$ nanosheets are more powerful in transfer of conduction band electrons, and thus accelerate the hydrogen generation reaction.

4. Conclusion

This paper comes up with a novel structure of Ni(OH)$_2$ cocatalyst for the hydrogen generation from water splitting by CdS nanorods photocatalyst. Ultrathin Ni(OH)$_2$ nanosheets was prepared *via* facile chemical routine at room temperature with PVP served as capping reagent. Under the same photo-catalytic reaction conditions and their respective optimal loading amount, the hydrogen generation rate of Ni(OH)$_2$/CdS is high up to 40.18 mmol h^{-1} g^{-1} with a quantum efficiency of 66.1% at 420 nm, 1.5 times as much as that of Pt/CdS. Time-resolved fluorescence show that Ni(OH)$_2$ NPs prolong the lifetime of band-edge emission electrons of CdS photocatalyst, which largely benefits to the promotion of separation efficiency of photo-induced charges, and finally results in the improvement of hydrogen generation rate. Ultrathin Ni(OH)$_2$ nanosheets provide much more reaction active cites, benefit to the transfer and separation of photo-reduced carriers, and result in the promotion of reaction rate. In addition, ultrathin materials often have atomic thickness, given them unique catalytic property, which significantly accelerate the hydrogen generation. Considering the low cost of Ni metal and its metal salts, ultrathin Ni(OH)$_2$ nanosheets cocatalyst connected with CdS nanorods photocatalyst undoubtedly shows commercial application.

Conflicts of interest

There are no conflicts to declare.

Acknowledgements

References

1 S. Chen, X.-P. Chen, Q.-Z. Jiang, J. Yuan, C.-F. Lin and W.-F. Shangguan, *Appl. Surf. Sci.*, 2014, **316**, 590–594.

2 S. Cao, C.-J. Wang, X.-J. Lv, Y. Chen and W.-F. Fu, *Appl. Catal., B*, 2015, **162**, 381–391.

3 T. Simon, N. Bouchonville, M. J. Berr, A. Vaneski, A. Adrović, D. Volbers, R. Wyrwich, M. Döblinger, A. S. Susha, A. L. Rogach, F. Jäckel, J. K. Stolarczyk and J. Feldmann, *Nat. Mater.*, 2014, **13**, 1013–1018.

4 X.-Y. Li, H. Wang, T.-T. Chu, D.-Z. Li and L.-Q. Mao, *Mater. Res. Bull.*, 2014, **57**, 254–259.

5 H. Wang, W. Chen, J. Zhang, C.-P. Huang and L.-Q. Mao, *Int. J. Hydrogen Energy*, 2015, **40**, 340–345.

6 W. Wang, S. Liu, L. Nie, B. Cheng and J. Yu, *Phys. Chem. Chem. Phys.*, 2013, **15**, 12033–12039.

7 E. P. Melián, M. N. Suárez, T. Jardiel, J. M. D. Rodrígueza, A. C. Caballero, J. Araña, D. G. Calatayud and O. G. Díaz, *Appl. Catal., B*, 2014, **152–153**, 192–201.

8 Y. Yamada, T. Miyahigashi, H. Kotani, K. Ohkubo and S. Fukuzumi, *Energy Environ. Sci.*, 2012, **5**, 6111–6118.

9 C. T. Dinh, M. H. Pham, F. Kleitz and T. O. Do, *J. Mater. Chem. A*, 2013, **1**, 13308–13313.

10 P. D. Tran, L.-F. Xi, S. K. Batabyal, L. H. Wong, J. Barber and J. S. C. Loo, *Phys. Chem. Chem. Phys.*, 2012, **14**, 11596–11599.

11 H. Husin, W.-N. Su, H.-M. Chen, C.-J. Pan, S.-H. Chang, J. Rick, W. T. Chuang, H. S. Sheu and B. J. Hwang, *Green Chem.*, 2011, **13**, 1745–1754.

12 X.-P. Chen, S. Chen, C.-F. Lin, Z. Jiang and W.-F. Shangguan, *Int. J. Hydrogen Energy*, 2015, **40**, 998–1004.

13 T. Sreethawong, Y. Suzuki and S. Yoshikawa, *Int. J. Hydrogen Energy*, 2005, **30**, 1053–1062.

14 S.-F. Chen, W. Zhao, W. Liu and S.-J. Zhang, *Appl. Surf. Sci.*, 2008, **255**, 2478–2484.

15 M. A. Ahmed, *J. Photochem. Photobiol., A*, 2012, **238**, 63–70.

16 X.-P. Chen, W. Chen, H.-Y. Gao, Y. Yang and W. F. Shangguan, *Appl. Catal., B*, 2014, **152–153**, 68–72.

17 M.-K. Tian, W.-F. Shangguan, J. Yuan, L. Jiang, M.-X. Chen, J.-W. Shi, Z.-Y. Ouyang and S.-J. Wang, *Appl. Catal., A*, 2006, **309**, 76–84.

18 J. Choi, S. Y. Ryu, W. Balcerski, T. K. Lee and M. R. Hoffmann, *J. Mater. Chem.*, 2008, **18**, 2371–2378.

19 S. Y. Ryu, J. Choi, W. Balcerski, T. K. Lee and M. R. Hoffmann, *Ind. Eng. Chem. Res.*, 2007, **46**, 7476–7488.

20 H.-Y. Lin, H.-C. Yang and W.-L. Wang, *Catal. Today*, 2011, **174**, 106–113.

21 J. Kim, D. W. Hwang, H. G. Kim, S. W. Bae, S. M. Ji and J. S. Lee, *Chem. Commun.*, 2002, **21**, 2488–2489.

22 W. Zhang, Y.-B. Wang, Z. Wang, Z.-Y. Zhong and R. Xu, *Chem. Commun.*, 2010, **46**, 7631–7633.

23 J.-L. Meng, F.-Y. Li, Y.-M. Hu, L. Xu, Z.-X. Sun and J. Liu, *Mater. Res. Bull.*, 2013, **48**, 2111–2116.

24 J. Zhang, S.-Z. Qiao, L.-F. Qi and J.-G. Yu, *Phys. Chem. Chem. Phys.*, 2013, **15**, 12088–12094.

25 J.-D. Hong, Y. S. Wang, Y.-B. Wang, W. Zhang and R. Xu, *ChemSusChem*, 2013, **6**, 2263–2268.

26 J. Zhang, L.-F. Qi, J.-R. Ran, J.-G. Yu and S.-Z. Qiao, *Adv. Energy Mater.*, 2014, **4**, 1301925–1301930.

27 L. Zhang, B.-Z. Tian, F. Chen and J. L. Zhang, *Int. J. Hydrogen Energy*, 2012, **37**, 17060–17067.

28 N.-X. Li, B.-Y. Zhou, P.-H. Guo, J.-C. Zhou and D.-W. Jing, *Int. J. Hydrogen Energy*, 2013, **38**, 11268–11277.

29 S. Devi, P. Korake, S. N. Achary and N. M. Gupta, *Int. J. Hydrogen Energy*, 2014, **39**, 19424–19433.

30 M. Tabata, K. Maeda, T. Ishihara, T. Minegishi, T. Takata and K. Domen, *J. Phys. Chem. C*, 2010, **114**, 11215–11220.

31 Y.-P. Yuan, S.-W. Cao, L.-S. Yin, L. Xu and C. Xue, *Int. J. Hydrogen Energy*, 2018, **38**, 7218–7223.

32 L.-S. Yin, Y.-P. Yuan, S.-W. Cao, Z.-Y. Zhang and C. Xue, *RSC Adv.*, 2014, **4**, 6127–6132.

33 J.-R. Ran, J.-G. Yu and M. Jaroniec, *Green Chem.*, 2011, **13**, 2708–2713.

34 J.-G. Yu, Y. Hai and B. Cheng, *J. Phys. Chem. C*, 2011, **115**, 4953–4958.

35 Z.-P. Yan, X.-X. Yu, A. Han, P. Xu and P.-X. Du, *J. Phys. Chem. C*, 2014, **118**, 22896–22903.

36 Y.-Z. Xia, S.-J. Liang, L. Wu and X.-X. Wang, *Catal. Today*, 2018, DOI: 10.1016/j.cattod.2018.03.061.

37 J.-R. Ran, J. Zhang, J.-G. Xu and S.-Z. Qiao, *ChemSusChem*, 2015, **7**, 3426–3434.

38 J.-G. Yu, S.-H. Wang, B. Cheng, Z. Lin and F. Huang, *Catal. Sci. Technol.*, 2013, **3**, 1782–1789.

39 J.-S. Jang, S. H. Choi, D. H. Kim, J. W. Jang, K. S. Lee and J. S. Lee, *J. Phys. Chem. C*, 2009, **113**, 8990–8996.

40 W. Chen, M.-C. Chu, L. Gao, L.-Q. Mao, J. Yuan and W.-F. Shanguan, *Appl. Surf. Sci.*, 2015, **324**, 432–437.

41 Z.-P. Yan, X.-X. Yu, Y.-Y. Zhang, H.-X. Jia, Z.-J. Sun and P.-W. Du, *Appl. Catal., B*, 2014, **160**, 173–178.

42 Y.-Z. Xia, W.-H. Chen, S.-J. Liang, J.-H. Bi, L. Wu and X.-X. Wang, *Catal. Sci. Technol.*, 2017, **7**, 5662–5669.

43 T.-Y. Peng, X.-H. Zhang, P. Zeng, K. Li, X.-G. Zhang and X.-G. Li, *J. Catal.*, 2013, **303**, 156–163.

44 Y. Xu and R. Xu, *Appl. Surf. Sci.*, 2015, **351**, 779–793.

45 X.-Q. Huang, S.-H. Tang, X.-L. Mu, Y. Dai, G.-X. Chen, Z.-Y. Zhou, F.-X. Ruan, Z.-L. Yang and N.-F. Zheng, *Nat. Nanotechnol.*, 2011, **6**, 28–32.

46 H.-H. Duan, N. Yan, R. Yu, C.-R. Chang, G. Zhou, H.-S. Hu, H.-P. Rong, Z.-Q. Niu, J.-J. Mao, H. Asakura, T. Tanka, P. J. Dyson, J. Li and Y.-D. Li, *Nat. Commun.*, 2014, **5**, 3093–3100.

47 A.-X. Yin, W.-C. Liu, J. Ke, W. Zhu, J. Gu, Y.-W. Zhang and C.-H. Yan, *J. Am. Chem. Soc.*, 2012, **134**, 20479–20489.

48 T.-T. Chu, H. Wang and L.-Q. Mao, *J. Mater. Eng. Perform.*, 2014, **23**, 3413–3417.

49 A. Nemamcha, J. L. Rehspringer and D. Khatmi, *J. Phys. Chem. B*, 2006, **110**, 383–387.

50 T.-J. Cai, M. Yue, X.-W. Wang, Q. Deng, Z.-S. Peng and W.-H. Zhou, *Chin. J. Catal.*, 2007, **28**, 10–16.

51 J.-W. Tang, Z.-G. Zou and J.-H. Ye, *J. Phys. Chem. B*, 2003, **107**, 14265–14269.

52 Q.-T. Pan, K. Huang, S.-B. Ni, Q. Wang, F. Yang and D.-Y. He, *Mater. Lett.*, 2007, **61**, 4773–4776.

53 L. Spanhel, M. Haase, H. Weller and A. Henglein, *J. Am. Chem. Soc.*, 1987, **109**, 5649–5655.

54 Y. Xu, W.-W. Zhao, R. Xu, Y.-M. Shi and B. Zhang, *Chem. Commun.*, 2013, **49**, 9803–9805.

55 Y.-j. S, H. Wang, J.-h. Xiong, B.-B. Guo, S.-J. Liang and L. Wu, *Appl. Catal., B*, 2018, **221**, 473–481.

56 G.-H. Cai, J.-P. Wang, X.-Q. Wu, Y.-Y. Zhan and S.-J. Liang, *Appl. Surf. Sci.*, 2018, **459**, 224–232.

57 Y. Huang, Y. Liu, D.-Y. Zhu, Y.-N. Xin and B. Zhang, *J. Mater. Chem. A*, 2016, **4**, 13626–13635.